=enter title here=

=list all authors here=

$^{=number=}$=Affiliation Address=

Key Points:

- enter point 1 here
- enter point 2 here
- enter point 3 here

Corresponding author: =name=, `=email address=`

Abstract
enter abstract here

1 Introduction

Slow slip events are a new feature discovered in the last two decades in many subduction zones thanks to recordings of the displacement of Earth's surface by dense Global Navigation Satellite System (GNSS) networks. As with ordinary earthquakes, slow slip events are caused by slip on a fault, such as the plate boundary between a tectonic plate subducting under another tectonic plate. However, they take a much longer time (several days to several years) to happen relative to ordinary earthquakes, and they have a relatively short recurrence time (months to years), compared to the recurrence time of regular earthquakes (up to several hundreds of years), allowing scientists to observe and study many complete event cycles, which is typically not possible to explore with traditional earthquake catalogs (Beroza & Ide, 2011). A slow slip event on the plate boundary is inferred to happen when there is a reversal of the direction of motion at GNSS stations, compared to the secular interseismic motion. Slow slip events have been observed in many subduction zones, such as Cascadia, Nankai (southwest Japan), Alaska, Costa Rica, Mexico, and New Zealand (Audet & Kim, 2016; Beroza & Ide, 2011).

In many places, tectonic tremor are also observed in relation to slow slip. Tremor is a long (several seconds to many minutes), low amplitude seismic signal, with emergent onsets, and an absence of clear impulsive phases. Tectonic tremor have been explained as a swarm of small, low-frequency earthquakes (LFEs) (Shelly, Beroza, & Ide, 2007), that is small magnitude earthquakes (M $\sim$ 1), for which frequency content (1-10 Hz) is lower than for ordinary earthquakes (up to 20 Hz). In subduction zones such as Nankai and Cascadia, tectonic tremor observations are spatially and temporally correlated with slow slip observations (Obara, 2002; Rogers & Dragert, 2003). Due to this correlation, these paired phenomena have been called Episodic Tremor and Slip (ETS). However, this is not always the case. For instance, in northern New Zealand, tremor are more challenging to detect, and seem to be located downdip of the slow slip on the plate boundary.

In Cascadia and Guerrero, Mexico, tremor has been used as a proxy to observe slow slip events that are not directly detectable in the GNSS data. For instance, Aguiar, Melbourne, and Scrivner (2009) computed the GPS-estimated moment release for 23 ETS events in Cascadia between 1997 and 2008. Simultaneously, they computed the cumulative number of hours of tectonic tremor recorded for each event. They observed a linear relationship between moment release and number of hours of tremor for ETS events of moment magnitude 6.3 to 6.8. For all these events, at least 50 hours of tectonic tremor where observed simultaneously with the GPS deformation. However, many smaller bursts of tremor of duration 1 to 50 hours were also observed in between the big ETS events. Based on the relationship between slow slip moment and number of hours of tremor, Aguiar et al. (2009) suggested that smaller slow slip events of magnitude 5-6 may occur simultaneously with the tremor bursts without being detectable in the GPS data.

Frank (2016) transformed the GPS time series into daily increments of surface motion by computing the first order differentiation of the time series. He then discarded the daily increments observed during known big slow slip events, and focused on the inter-events period. He divided the daily increments into two groups: the first group contains days when slow seismicity (tectonic tremor and LFEs) is detected, the second group contains days when the numbers of LFEs (for Guerrero) or tremor (for Cascadia) is lower than a threshold. He then stacked separately the two groups of daily increments and observed a cumulative displacement in the northern direction (for Guerrero) and the eastern direction (for Cascadia) corresponding to the loading period when few tremor or LFEs are observed and the surface deformation corresponds to the secular plate motion. He also observed a cumulative displacement in the southern direction (for Guerrero) and the western direction (for Cascadia) corresponding to the release period when tremor

and LFEs are observed. This reverse displacement corresponds to smaller slow slip events not directly observable in the GPS data.

However, in other subduction zones such as New Zealand, there is no clear relationship between tremor and slow slip occurrence and these methods cannot be applied. We thus need other methods to be able to better detect and quantify slow slip.

Wavelets methods such as the Discrete Wavelet Transform (DWT) are mathematical tools for analyzing time series simultaneously in the time and the frequency domain by observing how weighted averages of a time series vary from one averaging period to the next. Wavelet methods have been widely used for geophysical applications (Kumar & Foufoula-Georgiou, 1997). However, few studies have used wavelet methods to analyze recordings of slow slip, and their scope was limited to the detection of the bigger (magnitude 6-7) short-term (a few weeks) events.

Alba, Weldon, Livelybrooks, and Schmidt (2019) used hourly water level records from four tide gauges in the Juan de Fuca Straight and the Puget Sound to determine vertical displacements, uplift rates between ETS events, and net uplift rates between 1996 and 2011. The noise in the tide gauges data is associated with tides, and ocean and atmospheric noise on multiple timescales (a few days for storms to decades for oscillations between ocean basins), and is assumed to be coherent between each of the four tidal gauges studied. On the contrary, the uplift due to ETS events should be different at each tidal gauge. They first removed the tides using NOAA hourly harmonic tidal predictions. They then removed the residual noise using a method based on the DWT. More precisely, the authors applied a DWT to each of the four sites studied, and to the average of the four sites. Then, for each level of the DWT decomposition, they carried out a linear regression between the detail for one site and the detail for the average of the four sites. This process gives a coefficient for each level and for each site. They then constructed a noise signal for each site by multiplying the coefficient from the linear regression by the detail of the average over the four sites, and summing for all levels. The noise signal thus obtained was then removed from the time series. They then stacked multiple events to obtain an average event uplift rate, aligning the 12 ETS events using exact timing from GPS data. A difference in uplift between the two tidal gauges at Port Angeles and Port Townsend was then clearly seen in the stacked time series. Finally, the authors removed the long-term uplift rate and the long-term sea level rise to obtain an average inter-event uplift rate. They found that the inter-event deformation at a site is equal and opposite to the deformation during an ETS event, suggesting that ETS events are, on average, releasing the strain accumulated between ETS events.

Szeliga, Melbourne, Santillan, and Miller (2008) determined the timing and the amplitude of 34 slow slip events throughout the Cascadia subduction zone between 1997 and 2005. They stabilized the GPS time series using a reference set of stations from stable North America. They then modelled the GPS time series by the sum of a linear trend, annual and biannual sinusoids representing seasonal effects, and Heaviside step functions corresponding to earthquakes and hardware upgrades. The linear system was then solved using a weighted QR decomposition. Finally, they applied a Gaussian wavelet transform to the residual time series to get the exact timing of the slow slip at each GPS station. The succeeding wavelet basis functions are increasingly sensitive to temporal localization of a given signal, and the onset of faulting appears on the wavelet spectrum as an amplitude spike present over all frequencies. The offset for each slow slip event was then used to invert for the slow slip at depth by assuming a thrust fault slip at each subfault of the plate boundary. An equivalent moment magnitude was thus obtained.

Finally, instead of using wavelets in the time domain, Ohtani, McGuire, and Segall (2010) used 2D wavelet functions in the spatial domain to detect slow slip events. They designed the Network Stain Filter (NSF) to detect transient deformation signals from large-scale geodetic arrays. Contrary to their previous work on the Network Inversion Filter (NIF), there is no need to specify potential sources of deformation. They modeled the position of the GPS station by the sum of the secular velocity, a spatially coherent field, site-specific noise, reference frame errors, and observation errors. The spa-

tial displacement field is modeled by the sum of basis wavelets (the Deslauriers-Dubuc wavelet of degree 3) with time-varying weights. The transient is considered to be nearly steady-sate, so that it has spatial weights for the displacement and the velocity, but the acceleration is modeled by a random walk with a time-varying variance. All the time varying coefficients are estimated using Kalman filtering, and the optimization problem is regularized with the spatial sum of the transient strain rate field. Their method has been successfully used to detect a transient event in the Boso peninsula, Japan, and a slow slip event in the Alaska subduction zone (Wei, McGuire, & Richardson, 2012).

In this study, we use wavelet methods to analyze GPS and seismic recordings of slow slip events in Cascadia. Our objective is to verify that there is a good correlation between slow slip events detected with only GNSS data, and slow slip events detected with only seismic data. We thus want to demonstrate that the wavelet-based detection method can be applied to detect possible smaller (magnitude 5) slow slip events that may be currently undetected with standard methods.

2 Data

We focused our study on northwest Washington State. For the GNSS data, we used the GPS time series provided by the Pacific Northwest Geodetic Array, Central Washington University. These are network solutions in ITRF2008 with phase ambiguities resolved. Solutions are computed with JPL/NASA orbits and satellite clocks. North, East, and Vertical directions are available. However, as the direction of the secular plate motion is close to the East direction, we only used the East direction of the GPS time series for the data analysis, as it has the best signal-to-noise ratio. The wavelet method works best with data with zero mean, and no sharp discontinuities, so we use the cleaned dataset, that is GPS times eries with linear trends, steps due to earthquakes or hardware upgrades, and annual and semi-annual sinusoids signals simultaneously estimated and removed following Szeliga, Melbourne, Miller, and Santillan (2004). For the seismic data, we used the tremor catalog from the Pacific Northwest Seismic Network (PNSN) (Wech, 2010). Tremor were detected and located using waveform envelope correlation and clustering and a centroid location is available for every given five-minute time window when tremor was detected. As the catalog starts in August 2009, we only looked at GPS data recorded in 2009 or later.

3 Method

3.1 The Maximal Overlap Discrete Wavelet Transform

The Discrete Wavelet Transform (DWT) is an orthonormal transform that transforms a time series $X_t\,(t = 0, \cdots, N-1)$ into a vector of wavelet coefficients $W_i\,(i = 0, \cdots, N-1)$. If we denote J the level of the wavelet decomposition, and we have $N = n{*}2^J$, where n is some integer higher or equal to 1, the vector of wavelet coefficients can be decomposed into J wavelet vectors W_j of lengths $\frac{N}{2}$, $\frac{N}{4}$, ... , $\frac{N}{2^J}$, and one scaling vector V_J of length $\frac{N}{2^J}$. Each wavelet vector W_j is associated with changes on scale $\tau_j = dt2^{j-1}$, where dt is the time step of the time series, and corresponds to the filtering of the original time series with a filter with nominal frequency interval $[\frac{1}{dt2^{j+1}}; \frac{1}{dt2^j}]$. The scaling vector V_J is associated with averages in scale $\lambda_J = dt2^J$, and corresponds to the filtering of the original time series with a filter with nominal frequency interval $[0; \frac{1}{dt2^{j+1}}]$. We can also define for $j = 1, \cdots, J$ the jth wavelet detail D_j, which is a vector of length N, and is associated to scale $\tau_j = dt2^{j-1}$. Similarly, we can define for $j = 1, \cdots, J$ the jth wavelet smooth S_j, which is a vector of length N, and is associated to scales $\tau_{j+1} = dt2^{j+1}$ and higher. Together, the details and the smooths define the multiresolution analysis (MRA) of X:

$$X = \sum_{j=1}^{J} D_j + S_J \tag{1}$$

The DWT present several disadvantages. First, the length of the time series must be a multiple of 2^J where J is the level of the DWT decomposition. Second, the time step of the wavelet vector W_j is $dt2^j$, which may not correspond to the time when some interesting phenomenon is visible on the original time series. Third, when we circularly shift the time series, the corresponding wavelet coefficients, details and smooths are not a circularly shifted version of the wavelet coefficients, details and smooths of the original time series. Thus, the values of the wavelet coefficients, details and smooths are strongly dependent on the time when we start experimentally gathering the data. Finally, when we filter the time series to obtain the details and smooths, we introduce a phase shift, which makes difficult to line up meaningfully the features of the MRA with the original time series.

This is why we use instead the Maximal Overlap Discrete Wavelet Transform (MODWT). The MODWT transforms the time series $X_t\,(t = 0, ..., N-1)$ into J wavelet vectors $\widetilde{W}_j\,(j = 1, \cdots, J)$ of length N and a scaling vector $\widetilde{V}_J$ of length N. As is the case for the DWT, each wavelet vector $\widetilde{W}_j$ is associated with changes on scale $\tau_j = dt2^{j-1}$, and corresponds to the filtering of the original time series with a filter with nominal frequency interval $[\frac{1}{dt2^{j+1}}; \frac{1}{dt2^j}]$. The scaling vector $\widetilde{V}_J$ is associated with averages in scale $\lambda_J = dt2^J$, and corresponds to the filtering of the original time series with a filter with nominal frequency interval $[0; \frac{1}{dt2^{j+1}}]$. As is the case for the DWT, we can write the MRA:

$$X = \sum_{j=1}^{J} \widetilde{D}_j + \widetilde{S}_J \tag{2}$$

The MODWT of a time series can be defined for any length N. The time step of the wavelet vectors $\widetilde{W}_j$ and the scaling vector $\widetilde{V}_J$ is equal to the time step of the original time series. When we circularly shift the time series, the corresponding wavelet vectors, scaling vector, details and smooths are shifted by the same amount. The details and smooths are associated with a zero phase filter, making it easy to line up meaningfully the features of the MRA with the original time series. The wavelet methods for time series analysis are explained in a more detailed way in Percival and Walden (2000)).

3.2 Application to synthetic data

To illustrate the wavelet transform method, we first apply the MODWT to synthetics data. As slow slip events occur in Cascadia on a regular basis, every twelve to eighteen months, we create a synthetic signal of period $T = 500$ days. To reproduce the ground displacement observed on the longitudinal component of GPS stations in Cascadia, we divide each period into two parts: In the first part of duration $T-N$, the displacement is linearly increasing and corresponds to the secular plate motion in the eastern direction; in the second part of duration N, the displacement is linearly decreasing and corresponds to a slow slip event on a reverse fault at depth triggering a ground displacement in the western direction. To see the effect of the magnitude of the slow slip event, we use different values for $N = 2, 5, 10, 20$ days. Figure 1 shows the synthetics, the details of the wavelet decomposition for levels 1 to 8, and the smooth for the four durations of a slow slip event.

The ramp-like signal is transformed through the wavelet filtering into a waveform with first a positive peak and then a negative peak. The width of the waveform increases with the scale level. For the 8th level of the wavelet decomposition, the width of the waveform is nearly as large as the time between two events. We do not show details at larger scales as the corresponding waveforms would start to merge two contiguous events to-

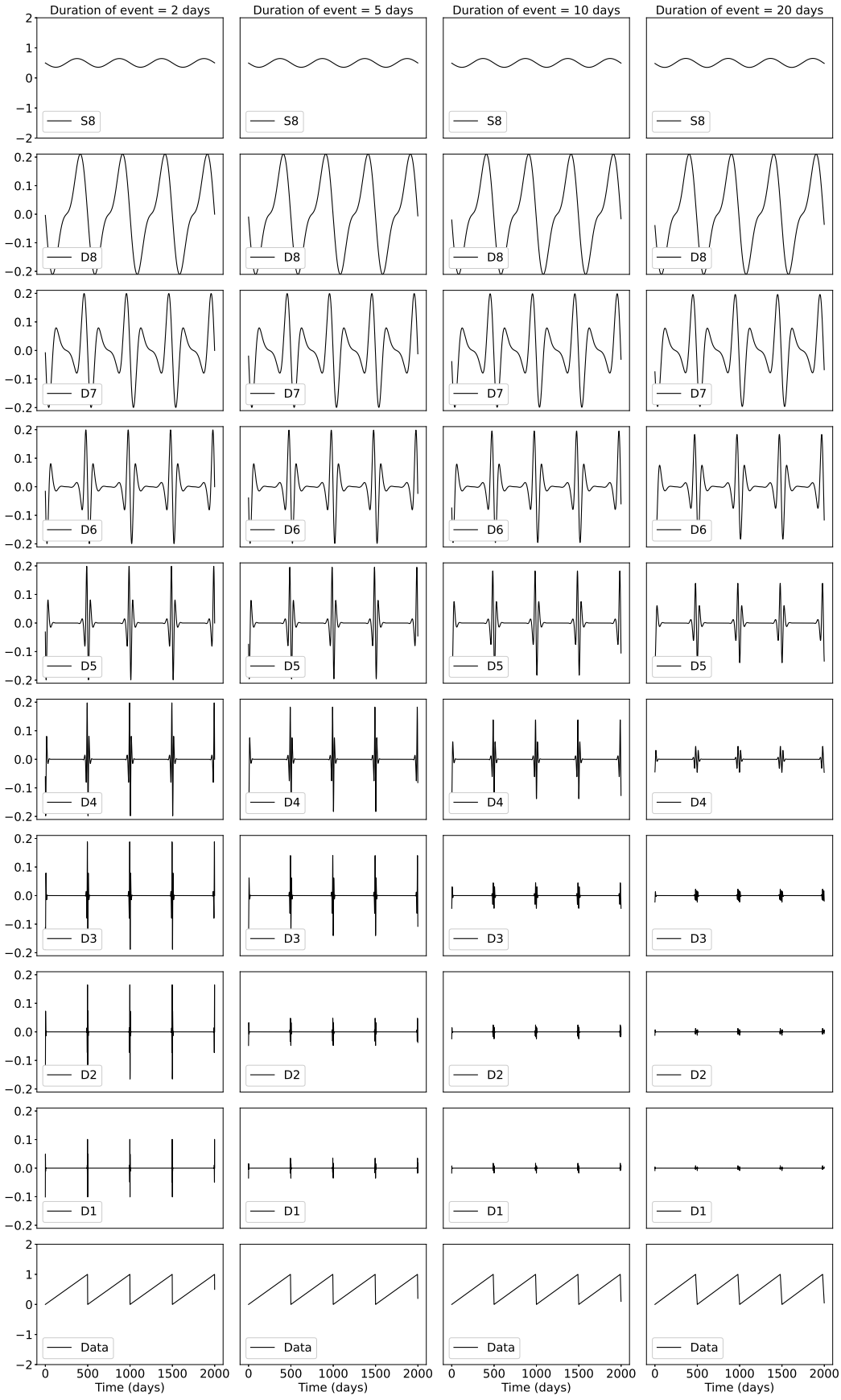

Figure 1. Details and smooth of the wavelet decomposition of a synthetics signal with period 500 days and duration of the slow slip event equal to 2 days (left), 5 days, 10 days, and 20 days (right).

gether, and make the wavelet decomposition less interpretable. For an event of duration 2 days, the wavelet details at levels higher than 2 have a larger amplitude than the wavelet detail at level 1. For an event of duration 5 days, the wavelet details at levels higher than 3 have a larger amplitude than the wavelet details at lower scales. For an event of duration 10 days, the wavelet details at levels higher than 5 have a larger amplitude than the wavelet details at lower scales. For an event of duration 20 days, the wavelet details at levels higher than 6 have a larger amplitude than the wavelet details at lower scales. Thus, the scale levels at which an event is being seen in the wavelet details give us an indication about the duration (and the magnitude) of the slow slip event. We expect the big slow slip events of magnitude 6-7 that lasts about 10 days to start being visible at the level 5 of the wavelet decomposition, but to not be noticeable at lower time scales.

3.3 MODWT of GPS and tremor data

4 Results

Explanation vespagram

Correlation

5 Discussion

6 Conclusion

Acknowledgments

Enter acknowledgments, including your data availability statement, here.

References

Aguiar, A., Melbourne, T., & Scrivner, C. (2009). Moment release rate of Cascadia tremor constrained by GPS. *Journal of Geophysical Research*, *114*, B00A05.

Alba, S., Weldon, R. J., Livelybrooks, D., & Schmidt, D. A. (2019). Cascadia ETS events seen in tidal records (1980–2011). *Bulletin of the Seismological Society of America*.

Audet, P., & Kim, Y. (2016). Teleseismic constraints on the geological environment of deep episodic slow earthquakes in subduction zone forearcs: A review. *Tectonophysics*, *670*, 1-15.

Beroza, G., & Ide, S. (2011). Slow earthquakes and nonvolcanic tremor. *Annual Review of Earth and Planetary Sciences*, *39*, 271-296.

Frank, W. (2016). Slow slip hidden in the noise: The intermittence of tectonic release. *Geophysical Research Letters*, *43*, 10125-10133.

Kumar, P., & Foufoula-Georgiou, E. (1997). Wavelet analysis for geophysical applications. *Reviews of Geophysics*, *35*(4), 385-412.

Obara, K. (2002). Nonvolcanic deep tremor associated with subduction in southwest Japan. *Science*, *296*(5573), 1679-1681.

Ohtani, R., McGuire, J., & Segall, P. (2010). Network strain filter: A new tool for monitoring and detecting transient deformation signals in GPS arrays. *Journal of Geophysical Research*, *115*, B12418.

Percival, D., & Walden, A. (2000). *Wavelet Methods for Time Series Analysis*. New York, NY, USA: Cambridge University Press.

Rogers, G., & Dragert, H. (2003). Tremor and slip on the Cascadia subduction zone: The chatter of silent slip. *Science*, *300*(5627), 1942-1943.

Shelly, D., Beroza, G., & Ide, S. (2007). Non-volcanic tremor and low-frequency earthquake swarms. *Nature*, *446*, 305-307.

Szeliga, W., Melbourne, T., Miller, M., & Santillan, V. (2004). Southern Cascadia

episodic slow earthquakes. *Geophysical Research Letters*, *31*, L16602.

Szeliga, W., Melbourne, T., Santillan, M., & Miller, M. (2008). GPS constraints on 34 slow slip events within the Cascadia subduction zone, 1997-2005. *Journal of Geophysical Research*, *113*, B04404.

Wech, A. (2010). Interactive tremor monitoring. *Seismological Research Letters*, *81*(4), 664-669.

Wei, M., McGuire, J., & Richardson, E. (2012). A slow slip event in the south central Alaska Subduction Zone. *Geophysical Research Letters*, *39*, L15309.